Journal of Medical Imaging

MedicalImaging.SPIEDigitalLibrary.org

# Assessment of natural enamel lesions with optical coherence tomography in comparison with microfocus x-ray computed tomography

Jorge Espigares
Alireza Sadr
Hidenori Hamba
Yasushi Shimada
Masayuki Otsuki
Junji Tagami
Yasunori Sumi

SPIE.

# Assessment of natural enamel lesions with optical coherence tomography in comparison with microfocus x-ray computed tomography

**Jorge Espigares,[a] Alireza Sadr,[b,c,*] Hidenori Hamba,[a] Yasushi Shimada,[a] Masayuki Otsuki,[a] Junji Tagami,[a] and Yasunori Sumi[d]**

[a]Tokyo Medical and Dental University, Department of Restorative Sciences, Cariology and Operative Dentistry, 1-5-45 Yushima, Bunkyo-ku, Tokyo 113-8549, Japan
[b]University of Washington School of Dentistry, 1959 NE Pacific Street, Seattle, Washington 98195, United States
[c]Tokyo Medical and Dental University, International Exchange Center, 1-5-45 Yushima, Bunkyo-ku, Tokyo 113-8549, Japan
[d]National Center for Geriatrics and Gerontology, National Hospital for Geriatric Medicine, Department of Advanced Medicine, Division of Oral and Dental Surgery, 36-3, Gengo, Morioka, Obu, Aichi 474-8511, Japan

**Abstract.** A technology to characterize early enamel lesions is needed in dentistry. Optical coherence tomography (OCT) is a noninvasive method that provides high-resolution cross-sectional images. The aim of this study is to compare OCT with microfocus x-ray computed tomography ($\mu$CT) for assessment of natural enamel lesions *in vitro*. Ten human teeth with visible white spot-like changes on the enamel smooth surface and no cavitation (ICDAS code 2) were subjected to imaging by $\mu$CT (SMX-100CT, Shimadzu) and 1300-nm swept-source OCT (Dental SS-OCT, Panasonic Health Care). In $\mu$CT, the lesions appeared as radiolucent dark areas, while in SS-OCT, they appeared as areas of increased signal intensity beneath the surface. An SS-OCT attenuation coefficient based on Beer–Lambert law could discriminate lesions from sound enamel. Lesion depth ranged from 175 to 606 $\mu$m in SS-OCT. A correlation between $\mu$CT and SS-OCT was found regarding lesion depth ($R = 0.81$, $p < 0.001$) and also surface layer thickness ($R = 0.76$, $p < 0.005$). The images obtained clinically in real time using the dental SS-OCT system are suitable for the assessment of natural subsurface lesions and their surface layer, providing comparable images to a laboratory high-resolution $\mu$CT without the use of x-ray.  [DOI: 10.1117/1.JMI.2.1.014001]

Keywords: optical coherence tomography; tissue characterization; x-ray imaging; dentistry; optical properties; enamel.

Paper 14141R received Oct. 24, 2014; accepted for publication Jan. 12, 2015; published online Feb. 11, 2015.

## 1 Introduction

Early detection of dental caries before breakdown of the enamel surface (cavitation) has become increasingly important in modern dentistry.[1,2] In order to perform a non- or minimally invasive treatment approach, assessment and monitoring of these lesions are essential. Hence, a noninvasive technology that can quantify characteristics of hidden or sub-surface caries such as lesion depth, surface layer thickness, and mineral changes over time is needed in dentistry. Dental radiographs do not have the sensitivity for detection of early carious lesions and are not considered to be suitable for monitoring purposes.[3]

Several other technologies have become available for enamel evaluation purposes based on quantified fluorescence, electrical conductivity, and near-infrared imaging;[4] however, a tool that can provide high-resolution cross-sectional images is still in demand. Optical coherence tomography (OCT) is a noninvasive and nondestructive diagnostic method that provides such images[5] and has been suggested as a useful modality for imaging dental caries.[6–9] The OCT does not use ionizing radiation, which is highly desirable. In OCT, a coherent light is projected over the sample, and the image is reconstructed in real time from depth-resolved backscattering. Performing multiple axial measurements of echo time delay called Axial scans or A-scans generates the cross-sectional images. Several A-scans along the sample can make a B-scan or tomographic image, and a series of B-scans become into a three-dimensional (3-D) reconstruction. The conventional OCT imaging system was based on the time-domain principle (TD-OCT), where a mirror mechanically scanned a distance at the reference arm to enable resolving of the depth information; more recently, spectral-domain OCT (or Fourier domain) systems have been developed. In these systems, instead of shifting the reference mirror, a stationary mirror is used and the images are obtained in a shorter time,[10] increasing the utility of OCT as a tool for clinical dentistry. A swept-source OCT (SS-OCT) system has been developed as one of the most recent implements of spectral discrimination, in which a tunable laser light source sweeps the near-IR wavelength at a high rate. SS-OCT time-encodes the wavelength, the images are obtained in almost real time and have a higher signal-to-noise ratio (SNR) compared with the TD-OCT.[11,12]

OCT is capable of assessing demineralization based on two main principles: increased light scattering in the porous demineralized tissue and depolarization of the incident light by the demineralized tissue. For the second one, polarization-sensitive OCT (PS-OCT) is required. By measuring the polarization properties of a sample in addition to reflectivity, PS-OCT provides a possibility for quantitative measurement of lesion severity. Both

*Address all correspondence to: Alireza Sadr, E-mail: alireza.ope@tmd.ac.jp

2329-4302/2015/$25.00 © 2015 SPIE

conventional and PS-OCT systems can observe demineralization as increased signal intensity. Image analysis techniques are based on this to quantify parameters such as lesion depth (as a cut-off point) and mineral loss (dB values integrated versus depth) in demineralized lesions. The potential of PS-OCT for determination of lesion structure, such as surface layer, has also been demonstrated.[7,13] However, to date the PS-OCT imaging system has been mainly based on the principles of TD-OCT, while the currently available SS-OCT systems are nonpolarization sensitive. Apparently, the optical setup of the conventional SS-OCT is more affordable compared with PS-OCT, because PS-OCT has a more complicated system. It should be noted that an SS-OCT system with cross-polarization (CP-OCT) capability has been introduced,[14,15] but it was reported that the lesion contrast in the PS-OCT system was superior when compared with the commercially available CP-OCT system.[16] On the other hand, a conventional high-resolution SS-OCT system has also the ability to observe gaps and defects in dental restorations and to evaluate resins composites' adaptation due to the high contrast images produced with the nonpolarized setup.[17–19] A prototype system with an intraoral probe has been available for dental use based on the SS-OCT system.[20–22]

Microfocus x-ray computed tomography ($\mu$CT) is a modified version of medical computed tomography that can achieve high-resolution images. This method is also nondestructive and provides analytical data in three dimensions *in vitro*. Analytical methods have been developed to quantitatively measure the mineral concentration of bones and teeth using $\mu$CT data. $\mu$CT is capable of characterizing and quantifying mineral densities of sound enamel and dentin; carious enamel and dentin; and demineralization and remineralization.[23] Differences in the linear attenuation coefficient of an x-ray beam passing through the sample at different viewing angles are responsible for x-ray image contrast, which allows quantitative analyses to be made.

As an early enamel lesion, white spot enamel lesions (WSELs) were defined as the stage of the caries process, prior to cavitation, where mineral has been lost from the enamel subsurface, with an intact surface layer overlying the mineral-poor region.[24] WSELs have been investigated by laboratory techniques such as transverse microradiography (TMR),[25,26] confocal microscopy,[27] and $\mu$CT.[28,29] Previous studies have reported on characterization of early enamel lesions by conventional OCT,[30,31] but they have mainly focused on artificial caries lesions rather than natural WSELs that develop nonuniformly. Moreover, conventional OCT images of natural enamel lesions have never been compared with those of $\mu$CT. OCT can be used in clinical situations, whereas in $\mu$CT, this is not possible. Therefore, the aim of this study is to check whether or not a clinical device with no ionizing radiation as SS-OCT is comparable with a laboratory high-resolution $\mu$CT in terms of WSEL assessment. The null hypothesis was that there was no significant correlation between SS-OCT and $\mu$CT measurements of enamel lesion parameters: lesion depth and surface layer thickness.

## 2 Materials and Methods

### 2.1 *Preparation of the Samples*

Ten extracted human permanent teeth with visible white spot-like changes on enamel smooth surface with no visible cavitation were selected. The lesions were carefully inspected by a clinician and met the criteria of International Caries Detection and Assessment System (ICDAS) code 2 corresponding with distinct visual changes in enamel.[32] These teeth were molars, and were mostly third molars. WSELs were placed in buccal or proximal surfaces. The teeth were collected from the Tokyo Medical and Dental University Hospital and the Institutional Review Board of TMDU approved their usage. They were cleaned and stored in distilled water at 4°C, with 0.1% thymol.

The cross-section of interest was marked using two guiding holes at the sides of the lesion; one apical and another one incisal to the lesion, each 2 mm from the visible borders of the lesion. The holes were created by Er:YAG laser (Erwin AdvErl; Morita, Tokyo, Japan) with the C400F tip. One pulse of 350 mJ was applied for each guiding hole.

Optical microscope images of the lesions were taken with a light stereo microscope at 1.5× magnification at objective lens (SM1000; Nikon, Tokyo, Japan). The roots of the teeth were removed at the level of the cementoenamel junction by means of a model trimmer (Y-230; Yoshida, Tokyo, Japan) and the crowns were analyzed.

### 2.2 $\mu$CT *System*

Each sample was then mounted on the computer-controlled turntable of a $\mu$CT system (InspeXio SMX-100CT; Shimadzu, Kyoto, Japan), so that the x-ray beam was perpendicular to the facial surface of the tooth. A schematic of the $\mu$CT setup is shown in Fig. 1. The 0.5-mm-thick aluminum and 0.3-mm-thick copper (0.5Al/0.3Cu) metal filters were placed in front of the detector for hardware beam hardening correction. These filters were used with software beam-hardening correction. X-rays were generated at a voltage of 100 kV/165 $\mu$A. To minimize ring artifacts, air calibration of the detector was carried out prior to each scanning. A 12-frame averaging was also applied in the acquisition phase to improve the SNR. Each tooth was rotated 360 deg within an integration time of 10 min. Data were acquired as 500 TIFF files for reconstruction of the 3-D image of the coronal part with $1024 \times 1024$ pixel resolution and 12-$\mu$m isotropic voxel sizes[33] [Fig. 1(a)]. For mineral density calibration, a series of mineral reference phantoms was also scanned, which included three hydroxyapatite (HAp) disks (Ratoc, Tokyo, Japan) with different concentrations of HAp crystals (0.20, 0.50, and 0.70 $g_{HAp}$ $cm^{-3}$) embedded in epoxy resin and an aluminum wire of 0.9 mm in thickness (equivalent to 3.55 $g_{HAp}$ $cm^{-3}$). CT values were converted into mineral values using a linear calibration curve, based on the gray values obtained from the mineral reference phantoms (linear regression, $R^2 > 0.99$).[29,33]

### 2.3 $\mu$CT *Image Analysis*

3-D image analysis software (TRI/3D-BON; Ratoc), originally developed for bone morphometry, was used for visualization and cropping the cross-section of interest.[33] An average image of the cross-section marked by the guiding holes was obtained over approximately 20-$\mu$m thickness, and a region of interest (ROI, width 240 $\mu$m × depth 1500 $\mu$m) from the surface of enamel to deeper levels was selected. When the lesion was too extensive, three ROIs were selected: incisal, middle, and apical. This was then converted to a mineral density-depth profile, considering 87 vol% maximum mineral in sound enamel.[24,33] These profiles were used to produce the following measurements: lesion depth ($LD_{\mu CT}$), the mineral loss ($\Delta Z$), thickness

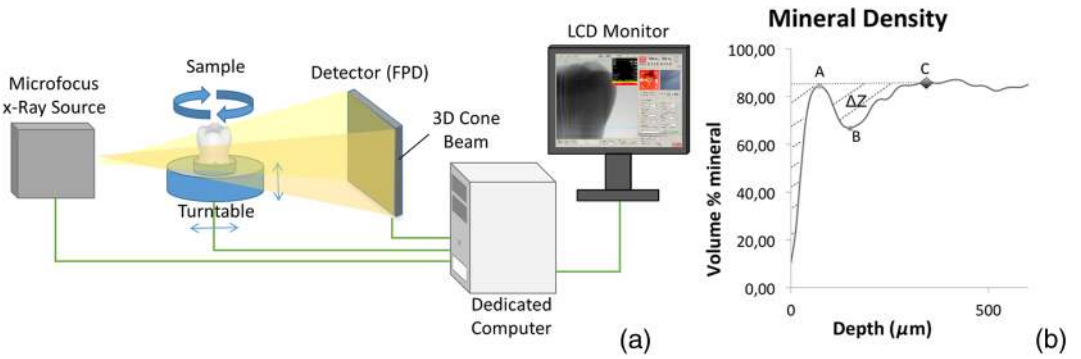


**Fig. 1** (a) Microfocus x-ray computed tomography ($\mu$CT) setup used in this study. (b) In the mineral density profile, the following points were marked: the maximum mineral content (A), minimum mineral content (B), and the start of sound enamel (C). These points were used for producing the following measurements: lesion depth, the mineral loss ($\Delta Z$), and thickness of surface layer (0-A). The start of the lesion was defined as the point where the mineral content was 20% that of the sound enamel.[34]

of surface layer ($SL_{\mu CT}$), and maximum mineral density at the surface layer, as in Fig. 1(b).

The surface layer is the intact layer overlying the subsurface lesion and represents the changes from the surface to the subsurface lesion. Its thickness was measured according to the method defined for TMR in 1975 by Groeneveld and Arends; from the start of the lesion to the maximum point of mineral density.[25,28]

On each of the 10 teeth, a cross-section of the visually sound enamel area was also obtained and analyzed by the same procedure as described above. Each area was selected from the cervical area of the corresponding tooth.

## 2.4 *SS-OCT System and Imaging*

The samples were then subjected to SS-OCT imaging (Dental OCT Prototype II, Panasonic Health Care) that incorporates a high-speed frequency-swept external cavity laser with the center wavelength of 1330 nm and bandwidth of 100 nm (Fig. 2). The axial and lateral resolutions of the system in air were 12 and 20 $\mu$m, respectively. The system acquired the image data (B-scan) in video rate. The imaging range in this study was 7 mm (width) by 7 mm (depth), forming a $2001 \times 1019$ pixel image.

The SS-OCT handheld scanning probe was set at 5-cm distance from the samples, with the scanning beam oriented about

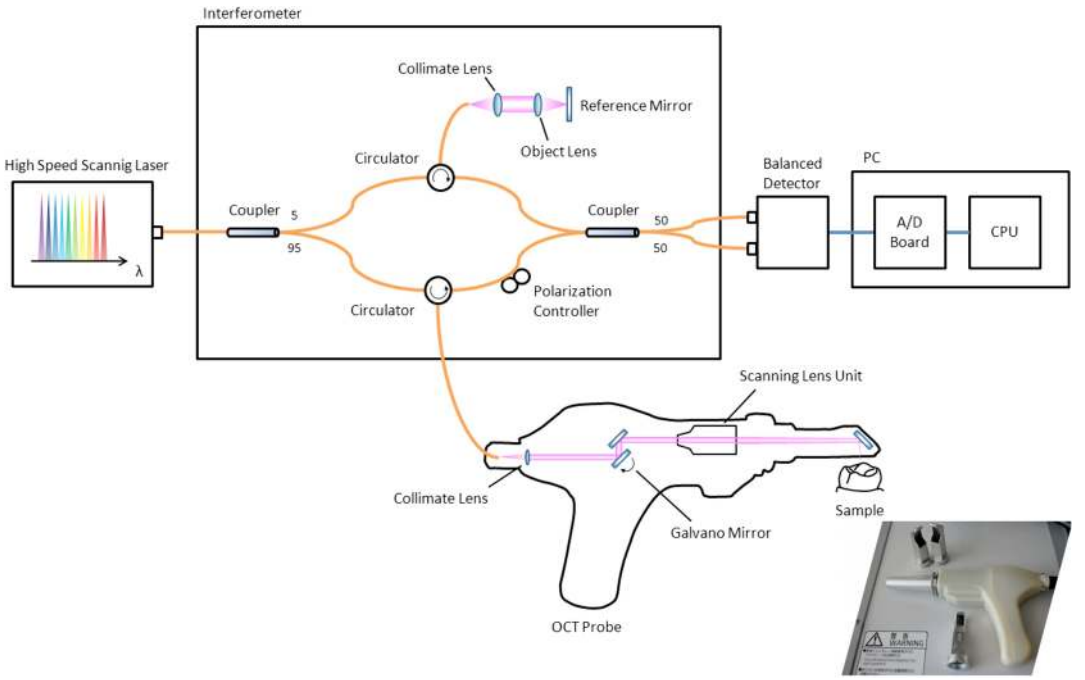


**Fig. 2** Swept-source OCT (SS-OCT) setup in this study; the output from a high-speed scanning laser is divided into reference arm and sample arm with a fiber splitter. Reference light and backscattered light from the sample are recombined with a second fiber coupler to create the interferogram in time. Fringe response is detected with a balanced detector, converted to electrical signal, and digitized by analog-to-digital (A/D) board. A PC software constructs a two-dimensional (2-D) image from the signal after Fourier transform. The inset shows the actual handheld probe with a set of metallic mouthpieces (straight and contra-angle) for intraoral imaging.

90 deg to the surface. The sample was mounted on a stage. Two-dimensional (2-D) sections at the exact point following the guiding holes were used. Since hydration significantly affects the SS-OCT signal intensity, the scans were performed in controlled hydrated condition after blot drying of the surface using a cotton pellet to leave the surface moist with no visible water droplets.

### 2.5 *SS-OCT Image Analysis*

For image analysis, a custom code in the image analysis software (ImageJ version 1.47V; Wayne Rasband, NIH, Bethesda, Maryland) was used to read the SS-OCT raw data of the section of interest. A noise reducing median filter (size 2) was applied to the data.[31] The analysis was performed at the same ROI as in $\mu$CT on a single B-scan, which would include data from a 20-$\mu$m-thick cross-section of the sample, corresponding to the SS-OCT beam spot size. Then, the intensity threshold value was adjusted to the depth of the visible boundary of the lesions. Values of boundary depth ($BD_{OCT}$) were obtained at each ROI. In addition, an attenuation coefficient ($\mu_t$) was calculated at each region to discriminate sound enamel from WSEL. $\mu_t$ is calculated on each average signal intensity profile based on the exponential decay of irradiance from the surface, using the equation derived from Beer–Lambert law, in the following equation:[31]

$$I(z) = ce^{-2u_t z}, \tag{1}$$

where $I$ is the reflectivity signal intensity in dB, $c$ is a constant, and $z$ is the depth variable. $\mu_t$ was calculated using linear least-squares regression to fit the natural log of average OCT profiles obtained from the ROI, as in Eq. (2):

$$\mu_t \propto -\frac{\ln I(z)}{2z}. \tag{2}$$

The surface layer thickness ($SL_{OCT}$), when visible as a low scattering transparent layer was measured using ImageJ. Four measurements of the $SL_{OCT}$ were taken and the average was used for comparison with the $\mu$CT values.

The resulting values obtained through SS-OCT were the optical values. In order to obtain the real ones, we divided them by 1.55, which is the average refractive index ($n$) of demineralized enamel.[35]

Ten samples of sound enamel were also analyzed and registered by the same procedure described above. As in $\mu$CT, these samples were selected from the cervical area of each tooth and from the same ROI as that in $\mu$CT.

### 2.6 *Statistical Analysis*

The relationships of $LD_{\mu CT}$ versus $BD_{OCT}$, $SL_{\mu CT}$ versus $SL_{OCT}$, and $LD_{\mu CT}$ versus $\Delta Z$ were investigated using Pearson parametric correlation. $P$ values less than 0.05 were regarded as being statistically significant. The values calculated for $\mu_t$ on SS-OCT scans were compared between the sound area ($\mu_{t\text{-sound}}$) and WSEL ($\mu_{t\text{-WSEL}}$) using $t$-test, and a cut-off value was calculated using receive operative curve (ROC) analysis. Statistical analyses were performed using SPSS (version 17, SPSS Inc, Chicago, Illinois) statistical software.

## 3 Results and Discussion

In $\mu$CT, the demineralized areas appeared radiolucent. In the SS-OCT images, the lesions appeared as areas of increased signal intensity and scattering beneath the surface up to a certain depth. These high scattering zones on SS-OCT images matched the demineralized areas on $\mu$CT. The appearance of an enamel lesion on SS-OCT occurs because the backscatter signal intensity increases with demineralization due to scattering at the numerous microinterfaces created in the hard tissue by the dissolution process of mineral.[36,37]

Subsurface lesions could be confirmed with both systems and their shape and depth could be determined on the resulting images from $\mu$CT and SS-OCT, as shown in Fig. 3. Sound enamel areas on SS-OCT image appeared to show less attenuation of the signal up to the dentin-enamel junction (DEJ), so that the DEJ was clearly visible (Fig. 4). However, in the case of the lesion area, it was difficult to distinguish DEJ [Fig. 3(b)], owing to the strong attenuation of the beam through the demineralized enamel area. In the case of deeper lesions, random scattering was occasionally observed at deep enamel areas, even beyond DEJ, however, the boundary of the lesion (taken as the $BD_{OCT}$) was still clearly detected [Fig. 3(c)].

In order to mimic a clinical situation and the oral cavity, the scans were taken controlling the hydration. It has been shown that hydration affects the reflectivity of demineralized porous enamel in direct proportion to the lesion extent.[30] Other factors that could negatively affect the light propagation through the lesion are plaque and calculus, which should be removed before imaging.

$LD_{\mu CT}$ ranged from 144 to 660 $\mu$m with an average of $402 \pm 163$ $\mu$m, while $BD_{OCT}$ ranged from 175 to 606 $\mu$m with an average of $366 \pm 134$ $\mu m$. These values were very similar between SS-OCT and $\mu$CT and are consistent with the values found for natural WSELs by Hamba et al.[33] (150 to 950 $\mu$m) and the values found by Cochrane et al.[28] (275 to 845 $\mu$m). In that study, $\mu$CT results were strongly correlated with those of TMR.

In the present study, the SS-OCT $\mu_t$ values were also investigated. $\mu_{t\text{-WSEL}}$ values ranged from 0.92 to 3.61 $mm^{-1}$ ($1.98 \pm 0.73$), and $\mu_{t\text{-sound}}$ values ranged from 0.31 to 0.70 $mm^{-1}$ ($0.53 \pm 0.12$). Comparing $\mu_t$ values, a significant difference was found between sound and WSEL regions using Student's $t$-test ($p < 0.05$). A cut-off value of 0.8 $mm^{-1}$ was derived from ROC analysis to discriminate sound area from demineralization. Sound enamel strongly attenuates light in the visible range, but the magnitude of scattering at higher wavelengths is lower than in the visible range. In the near-infrared region around the 1300-nm wavelength sound enamel becomes highly transparent,[6] while at a smaller wavelength (e.g., 850 nm), sound enamel attenuates the signal and there is an effective imaging depth of around 100 $\mu$m.[38–40] It has been confirmed that the magnitude of light scattering in sound enamel is prominently less than dentin[8] and that $\mu_t$ decreases in sound enamel, decreasing the SS-OCT signal attenuation, and increases with demineralization, indicating a strong attenuation through the lesion.[31] In our study, we saw an increase of $\mu_t$ in WSEL, which is consistent with a previous report that suggested on the same artificial caries lesion, $\mu_t$ showed a good correlation with integrated hardness as a measure of mineral content changes by de/remineralization.[31] Such a parameter is thought to be useful for monitoring natural lesions over time using a nonpolarization-sensitive OCT system.[21]

Within the limitations of this *in vitro* study, the null hypothesis of this study was rejected. The lesions showed an $SL_{\mu CT}$ ranging from 54.7 to 109.4 $\mu$m ($83.5 \pm 14.5$). $SL_{OCT}$ ranged from 41 to 80 $\mu$m ($65.5 \pm 10.3$). A correlation between $\mu$CT

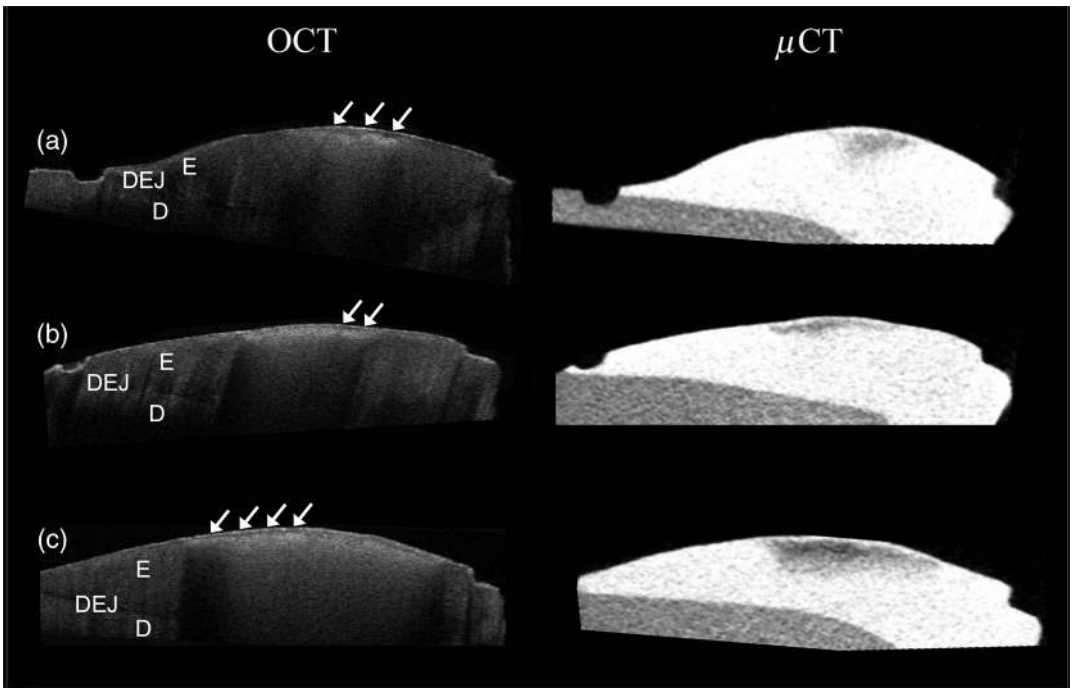


**Fig. 3** (a), (b) and (c) show a comparison of 2-D sections between SS-OCT and $\mu$CT. The lesions appear as high-scattering zones on SS-OCT, whereas on $\mu$CT the demineralized areas appear radiolucent. The arrows point to the visible surface layer overlying the subsurface lesion. The guiding holes made by laser ablation are visible on cross-sections from both SS-OCT and $\mu$CT. E, D, and DEJ show the enamel, dentin, and dentin-enamel junction, respectively.

and SS-OCT was found regarding lesion depth ($R = 0.81$, $p < 0.001$) and also surface layer thickness ($R = 0.76$, $p < 0.005$), when a distinct surface layer was visible with OCT, or in 7 of 10 cases (70%) (Fig. 5). In those cases, the layer appeared as a thin transparent layer overlying the high scattering zone.

It must be noted that the slope of regression line for the surface layer was different from 1, and SS-OCT tended to show smaller nominal readings than $\mu$CT. The reason should be attributed to the different methods used for defining surface layer in the two techniques (i.e., visible transparent layer in SS-OCT versus a theoretical parameter derived from mineral density profiles on $\mu$CT). Nevertheless, the correlation between these readings is an important finding despite different nominal values.

SS-OCT information is valuable especially with WSEL, where monitoring is highly desirable. The image analysis

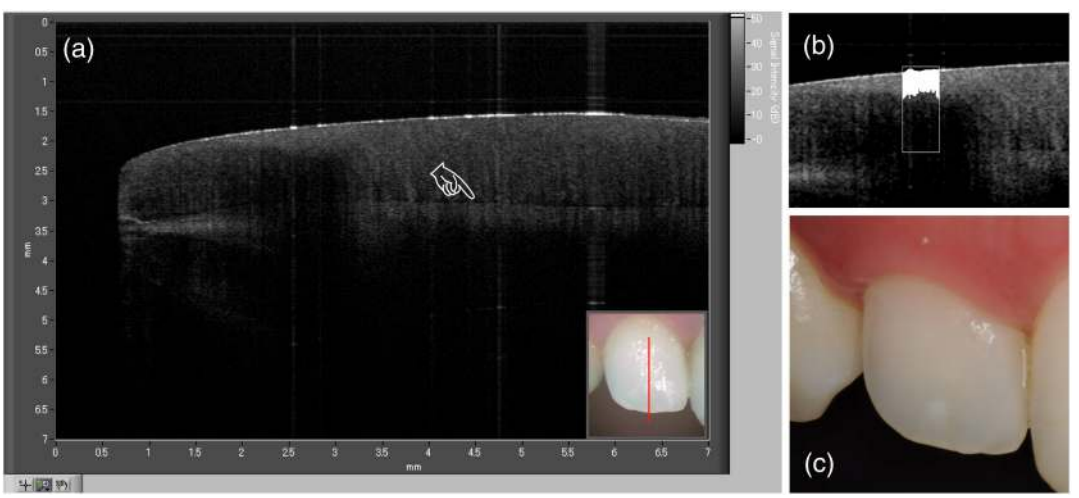


**Fig. 4** SS-OCT image obtained from a visible white spot lesion of upper right lateral incisor of a 32-year old volunteer male subject: (a) SS-OCT image as appearing on the screen, the inset is photographic image obtained in real time by the CMOS camera coupled with the laser beam at the imaging probe. (b) Image analysis of a region of interest in the center of the lesion suggested that in this clinical case, which appears to be a developmental hypocalcification, the $BD_{OCT}$ was 205 $\mu$m with a $SL_{OCT}$ of 60 $\mu$m. The attenuation coefficient ($\mu_t$) had a value of 2.14 $mm^{-1}$. (c) In a clinical photograph of the tooth, the lesion is visible. The finger pointer shows the visible DEJ.

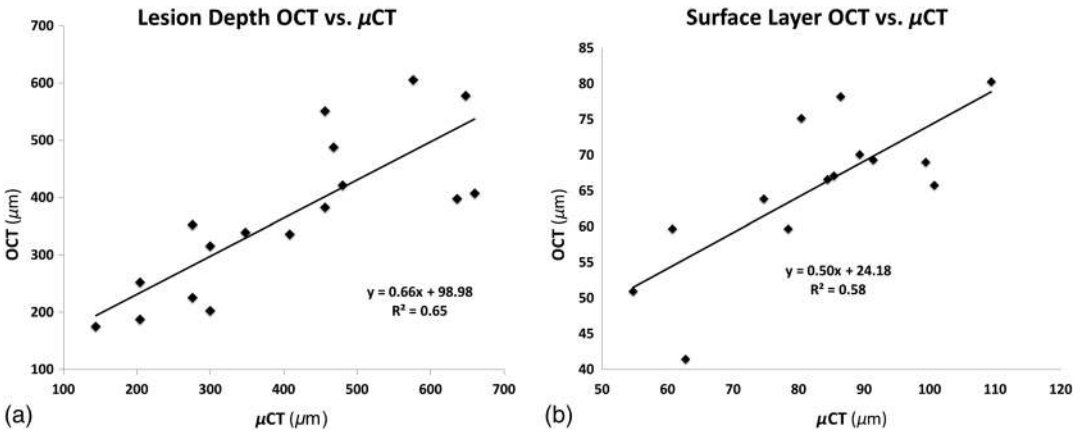


**Fig. 5** (a) SS-OCT and $\mu$CT lesion depth correlation ($R = 0.81$, $p < 0.001$), best regression was established with a linear fit ($R^2 = 0.65$). (b) SS-OCT and $\mu$CT surface layer correlation ($R = 0.76$, $p < 0.005$), linear regression ($R^2 = 0.58$). The surface layer was measured using the method of Groeneveld and Arends: from the start of the lesion to the point of maximum density.

approach taken in this study could effectively quantify lesion attributes. Such an approach is feasible for clinical images, as shown in the example presented in Fig. 4. On the other hand, due to the nature of $\mu$CT setup, this high-resolution modality cannot be used in clinical situations. Cone beam computed tomography could be used clinically; however, they do not have the resolution to detect early enamel demineralization.[41] Even if this improves in the future, the radiation dose (35 to 652 $\mu$Sv) makes it not the safest option for caries detection.[42,43] For comparison purposes, a single intraoral x-ray has an effective dose of 1 to 8 $\mu$Sv and a panoramic one 4 to 30 $\mu$Sv.

In the current study, only score 2 lesions were included, since they are rather deep and severe compared with score 1 lesions. The comparison of two modalities would have been more challenging on shallower lesions given their resolution being on the order of $>10$ $\mu$m; issues such as beam hardening and shadow artifacts make it difficult for current $\mu$CT systems to detect and characterize lesions that do not produce an adequate radiographic contrast to sound enamel due to their small amount of mineral loss. Nevertheless, assessment of the rather severe, yet noncavitated score 2 enamel lesions appears to be more critical in terms of clinical importance and monitoring.

One application of quantitative monitoring of such lesions would be in orthodontic treatments, where the accumulation of plaque is very frequent and can lead to the onset of WSELs.[14] Moreover, in previous studies, it was shown that existing WSELs can be treated via remineralization[44,45] or infiltration of low-viscosity resins materials.[46] Other examples involve remineralization efforts by fluoride application or newly introduced agents such as bioavailable calcium releasing chewing gums.[21] In this regard, removal of the surface layer is considered to be necessary for a proper penetration of the infiltrant into the lesion body.[27] The results of our study are in line with those previous reports suggesting that these highly mineralized layers appear similar to sound enamel under OCT.[47] The obtained surface layers were consistent in values with those obtained by Cochrane et al.;[28] generally 35 to 60 $\mu$m occasionally reaching 130 $\mu$m.

It is noteworthy that no correlation was found between the surface layer thickness and the lesion depth, meaning that the thicker surface layers are not necessarily associated with deeper lesions. However, a significant correlation was found between $LD_{\mu CT}$ and $\Delta Z$ ($R = 0.74$, $p < 0.005$), showing that the deeper lesions exhibited lower minimum mineral content in the body of the lesion, which is also consistent with a previous report.[28]

Although 2-D cross-sections were used for the analysis in this study, 3-D scans provided similar images to those coming from $\mu$CT (Fig. 6). Faster sources with high scanning speeds and microelectromechanical systems incorporated into the scanning probe enable clinical acquisition of such 3-D images in quasi-real time.[14] Nonetheless, there are still limitations for a full adoption of OCT for daily dental practice, which include the high cost of the device as a diagnostic/monitoring modality. A more compact design for the system as well as a smaller and more ergonomic probe would be desirable for a better intraoral maneuverability in a daily clinical use of this highly capable modality.

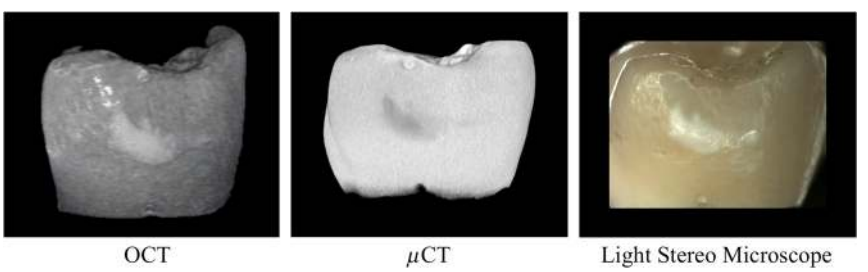


**Fig. 6** Three-dimensional (3-D) image of the same lesion by SS-OCT and $\mu$CT along with light stereo microscope image. The lateral spread of the lesion can be clearly seen on SS-OCT. The $\mu_t$ can be calculated from the SS-OCT signal over the volume of interest, in this case $1.42 \pm 0.16$ mm$^{-1}$.

## 4 Conclusion

Significant correlations were found between natural lesion parameters from SS-OCT and a laboratory high-resolution $\mu$CT. SS-OCT is a valid technology for clinical assessment of surface layer and depth of natural subsurface enamel lesions without the use of x-ray.

### Acknowledgments

This work was supported by grants-in-aid for scientific research Nos. 24792019 and 24592861 from the Japan Society for the Promotion of Science and the Ministry of Health Longevity Sciences Grant (21A-8).

### References

1. J. D. Featherstone, "The continuum of dental caries—evidence for a dynamic disease process," *J. Dent. Res.* **83**(Spec No C), C39–C42 (2004).
2. M. J. Tyas et al., "Minimal intervention dentistry—a review. FDI Commission Project 1–97," *Int. Dent. J.* **50**(1), 1–12 (2000).
3. R. Haak, M. J. Wicht, and M. J. Noack, "Conventional, digital and contrast-enhanced bitewing radiographs in the decision to restore approximal carious lesions," *Caries Res.* **35**(3), 193–199 (2001).
4. P. Rechmann, B. M. Rechmann, and J. D. Featherstone, "Caries detection using light-based diagnostic tools," *Compend. Contin. Educ. Dent.* **33**, 582–584, 586, 588–593; quiz 594, 596 (2012).
5. D. Huang et al., "Optical coherence tomography," *Science* **254**(5035), 1178–1181 (1991).
6. D. Fried et al., "Early caries imaging and monitoring with near-infrared light," *Dent. Clin. North Am.* **49**(4), 771–793, vi (2005).
7. D. Fried et al., "Imaging caries lesions and lesion progression with polarization sensitive optical coherence tomography," *J. Biomed. Opt.* **7**(4), 618–627 (2002).
8. D. Fried et al., "Nature of light scattering in dental enamel and dentin at visible and near-infrared wavelengths," *Appl. Opt.* **34**, 1278–1285 (1995).
9. Y. Chen et al., "Characterization of dentin, enamel, and carious lesions by a polarization-sensitive optical coherence tomography system," *Appl. Opt.* **44**(11), 2041–2048 (2005).
10. M. Yamanari et al., "Visualization of phase retardation of deep posterior eye by polarization-sensitive swept-source optical coherence tomography with 1-microm probe," *Opt. Express* **17**(15), 12385–12396 (2009).
11. M. Choma et al., "Sensitivity advantage of swept source and Fourier domain optical coherence tomography," *Opt. Express* **11**(18), 2183–2189 (2003).
12. Y. Yasuno et al., "Three-dimensional and high-speed swept-source optical coherence tomography for in vivo investigation of human anterior eye segments," *Opt. Express* **13**(26), 10652–10664 (2005).
13. P. Ngaotheppitak, C. L. Darling, and D. Fried, "Measurement of the severity of natural smooth surface (interproximal) caries lesions with polarization sensitive optical coherence tomography," *Lasers Surg. Med.* **37**(1), 78–88 (2005).
14. A. Nee et al., "Longitudinal monitoring of demineralization peripheral to orthodontic brackets using cross polarization optical coherence tomography," *J. Dent.* **42**(5), 547–555 (2014).
15. P. Lenton et al., "Clinical cross-polarization optical coherence tomography assessment of subsurface enamel below dental resin composite restorations," *J. Med. Imaging* **1**(1), 016001 (2014).
16. H. Kang, C. L. Darling, and D. Fried, "Nondestructive monitoring of the repair of natural occlusal lesions using cross-polarization optical coherence tomography," *Proc. SPIE* **8208**, 82080X (2012).
17. T. A. Bakhsh et al., "Non-invasive quantification of resin-dentin interfacial gaps using optical coherence tomography: validation against confocal microscopy," *Dent. Mater.* **27**(9), 915–925 (2011).
18. M. M. Mandurah et al., "Characterization of transparent dentin in attrited teeth using optical coherence tomography," *Lasers Med. Sci.* (2014).
19. T. A. Bakhsh et al., "Concurrent evaluation of composite internal adaptation and bond strength in a class-I cavity," *J. Dent.* **41**(1), 60–70 (2013).
20. Y. Shimada et al., "Noninvasive cross-sectional imaging of proximal caries using swept-source optical coherence tomography (SS-OCT) in vivo," *J. Biophotonics* **7**(7), 506–513 (2014).
21. A. Sadr et al., "Monitoring of enamel lesion remineralization by optical coherence tomography: an alternative approach towards signal analysis," *Proc. SPIE* **8566**, 856602 (2013).
22. Y. Nakajima et al., "Detection of occlusal caries in primary teeth using swept source optical coherence tomography," *J. Biomed. Opt.* **19**(1), 016020 (2014).
23. T. N. Clementino-Luedemann and K. H. Kunzelmann, "Mineral concentration of natural human teeth by a commercial micro-CT," *Dent. Mater. J.* **25**(1), 113–119 (2006).
24. J. Arends and J. Christoffersen, "The nature of early caries lesions in enamel," *J. Dent. Res.* **65**(1), 2–11 (1986).
25. A. Groeneveld and J. Arends, "Influence of pH and demineralization time on mineral content, thickness of surface layer and depth of artificial caries lesions," *Caries Res.* **9**(1), 36–44 (1975).
26. H. M. Theuns et al., "The surface layer during artificial carious lesion formation," *Caries Res.* **18**(2), 97–102 (1984).
27. H. Meyer-Lueckel, S. Paris, and A. M. Kielbassa, "Surface layer erosion of natural caries lesions with phosphoric and hydrochloric acid gels in preparation for resin infiltration," *Caries Res.* **41**(3), 223–230 (2007).
28. N. J. Cochrane et al., "An X-ray microtomographic study of natural white-spot enamel lesions," *J. Dent. Res.* **91**(2), 185–191 (2012).
29. T. T. Huang et al., "Characterisation of enamel white spot lesions using X-ray micro-tomography," *J. Dent.* **35**(9), 737–743 (2007).
30. A. Nazari et al., "Effect of hydration on assessment of early enamel lesion using swept-source optical coherence tomography," *J. Biophotonics* **6**(2), 171–177 (2013).
31. M. M. Mandurah et al., "Monitoring remineralization of enamel subsurface lesions by optical coherence tomography," *J. Biomed. Opt.* **18**(4), 046006 (2013).
32. A. Jablonski-Momeni et al., "Reproducibility and accuracy of the ICDAS-II for detection of occlusal caries in vitro," *Caries Res.* **42**(2), 79–87 (2008).
33. H. Hamba et al., "Enamel lesion parameter correlations between polychromatic micro-CT and TMR," *J. Dent. Res.* **91**(6), 586–591 (2012).
34. J. M. ten Cate et al., "Preparation and measurement of artificial enamel lesions, a four-laboratory ring test," *Caries Res.* **30**(6), 400–407 (1996).
35. I. Hariri et al., "Estimation of the enamel and dentin mineral content from the refractive index," *Caries Res.* **47**(1), 18–26 (2013).
36. Y. Natsume et al., "Estimation of lesion progress in artificial root caries by swept source optical coherence tomography in comparison to transverse microradiography," *J. Biomed. Opt.* **16**(7), 071408 (2011).
37. H. Nakagawa et al., "Validation of swept source optical coherence tomography (SS-OCT) for the diagnosis of smooth surface caries in vitro," *J. Dent.* **41**(1), 80–89 (2013).
38. M. G. Sowa et al., "A comparison of methods using optical coherence tomography to detect demineralized regions in teeth," *J. Biophotonics* **4**(11–12), 814–823 (2011).
39. S. Chung et al., "Multispectral near-IR reflectance and transillumination imaging of teeth," *Biomed. Opt. Express* **2**(10), 2804–2814 (2011).
40. D. P. Popescu et al., "Assessment of early demineralization in teeth using the signal attenuation in optical coherence tomography images," *J. Biomed. Opt.* **13**(5), 054053 (2008).
41. F. Haiter-Neto, A. Wenzel, and E. Gotfredsen, "Diagnostic accuracy of cone beam computed tomography scans compared with intraoral image modalities for detection of caries lesions," *Dentomaxillofac. Radiol.* **37**(1), 18–22 (2008).
42. J. A. Roberts et al., "Effective dose from cone beam CT examinations in dentistry," *Br. J. Radiol.* **82**(973), 35–40 (2009).
43. Z. L. Zhang et al., "The detection accuracies for proximal caries by cone-beam computerized tomography, film, and phosphor plates," *Oral. Surg. Oral. Med. Oral. Pathol. Oral. Radiol. Endod.* **111**(1), 103–108 (2011).
44. N. J. Cochrane et al., "New approaches to enhanced remineralization of tooth enamel," *J. Dent. Res.* **89**(11), 1187–1197 (2010).
45. Y. Kitasako et al., "Gum containing calcium fluoride reinforces enamel subsurface lesions in situ," *J. Dent. Res.* **91**(4), 370–375 (2012).

46. S. Paris and H. Meyer-Lueckel, "Inhibition of caries progression by resin infiltration in situ," *Caries Res.* **44**(1), 47–54 (2010).
47. Y. Iino et al., "Detection of a second mesiobuccal canal in maxillary molars by swept-source optical coherence tomography," *J. Endod.* **40**(11), 1865–1868 (2014).

**Jorge Espigares** is a second year PhD student at the University of Tokyo Medical and Dental University. He received his BDS degree in dentistry from the University of Granada, Spain, in 2005. His research project involves the image analysis and application of optical coherence tomography systems in clinical dentistry.

**Alireza Sadr** is an acting associate professor at the University of Washington School of Dentistry. Previously, he served Tokyo Medical and Dental University (TMDU) as a faculty member at the Global Center of Excellence. He received his PhD degree from TMDU in 2008. He is the author of more than 90 journal papers and his current research interests include restorative dentistry, dental materials, biophotonics, and optical coherence tomography in dentistry. He is a member of SPIE.

**Hidenori Hamba** is an assistant professor at Tokyo Medical and Dental University (TMDU). He received his PhD degree in dental science from TMDU in 2012. His current research interests include enamel de/remineralization and establishment of microcomputed tomography for mineral content assessment of dental hard tissue.

**Yasushi Shimada** is a senior faculty member of cariology and operative dentistry at Tokyo Medical and Dental University. He studied dentistry and took his PhD degree at this institution. His extended research activities have involved characterization of dental adhesives introducing new methodologies such as the wire-loop microshear bond strength test. He is currently involved in the dental OCT research project with a focus on the clinical aspect.

**Masayuki Otsuki** is an associate professor of cariology and operative dentistry at Tokyo Medical and Dental University, where he also received his PhD degree. His research interests have involved the application of various lasers including Er:YAG for ablation of dental tissues as well as accelerated tooth whitening.

**Junji Tagami** received his DDS degree in 1980 and PhD degree in 1984 from Tokyo Medical and Dental University. Currently, he is the chairman of Cariology and Operative Dentistry and a vice president of Tokyo Medical and Dental University. Following the principles of minimally invasive dentistry introduced by the late Prof. Fusayama, his primary research interests involve adhesion to tooth substance and the broad area of cariology.

**Yasunori Sumi** is the professor and director at the Division of Oral and Dental Surgery, Department of Advanced Medicine, National Center for Geriatrics and Gerontology. His primary research interest has focused on oral care for the elderly. He is a dental OCT research advocate and works with a number of coinvestigators in the OCT project funded by Research Grant for Longevity Sciences from Ministry of Health, Labor and Welfare.